Обзор ArXiv:astro-ph, за 3-7 апреля 2017

От Сильченко О.К.

Astro-ph: 1703.10782

Do AGN outflows quench or enhance star formation?

Kastytis Zubovas[1,2*] and Martin A. Bourne[3]

[1] *Center for Physical Sciences and Technology, Savanoriu 231, Vilnius LT-02300, Lithuania*
[2] *Astronomy Observatory, Faculty of Physics, Vilnius University, M. K. Čiurlionio 29, Vilnius LT-03100, Lithuania*
[3] *Institute of Astronomy and Kavli Institute for Cosmology, University of Cambridge, Madingley Road, Cambridge, CB3 0HA, UK*
* *E-mail:* kastytis.zubovas@ftmc.lt

3 April 2017

ABSTRACT

AGN outflows can remove large quantities of gas from their host galaxy spheroids, potentially shutting off star formation. On the other hand, they can compress this gas, potentially enhancing or triggering star formation, at least for short periods. We present a set of idealised simulations of AGN outflows affecting turbulent gas spheres, and investigate the effect of the outflow and the AGN radiation field upon gas fragmentation. We show that AGN outflows of sufficient luminosity shut off fragmentation while the nucleus is active, but gas compression results in a burst of fragmentation after the AGN switches off. Self-shielding of gas against the AGN radiation field allows

Включение на 1 млн лет активного ядра разной светимости
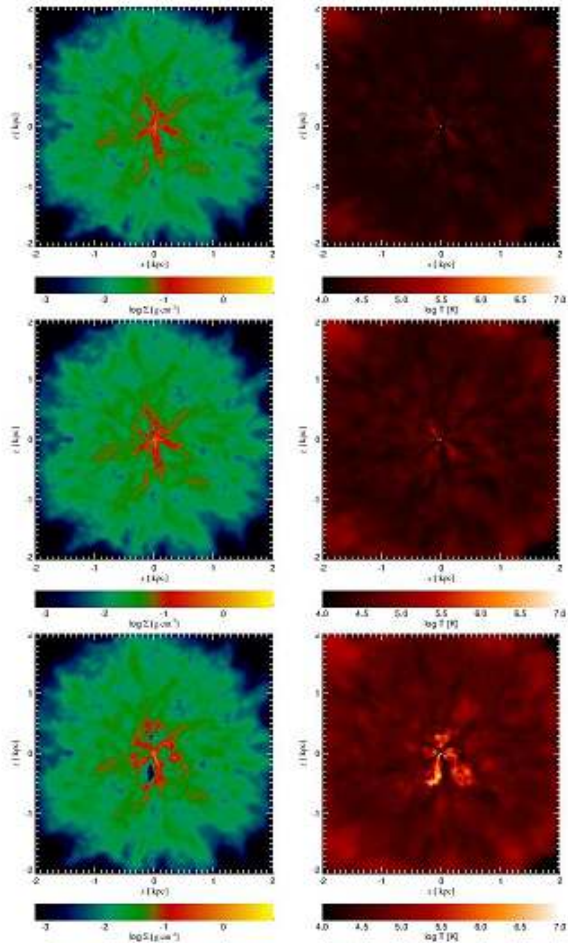
Figure 1. Density maps (left column), temperature maps (middle column), both at $t = 1$ Myr after the start of the AGN phase, and fragmentation rates over time in three of the seven simulations with $t_q = 1$ Myr. Fragmentation rate plots include the rates of a control simulation (dashed lines). Vertical dashed lines in the fragmentation rate plots show the start and end of the AGN phase. From top to bottom, the simulations have progressively higher values of AGN luminosity $L = L_{AGN}/(1.3 \times 10^{46} \mathrm{ergs}^{-1})$: $L = 0.5, 1, 2$. See below for simulations with higher luminosities.
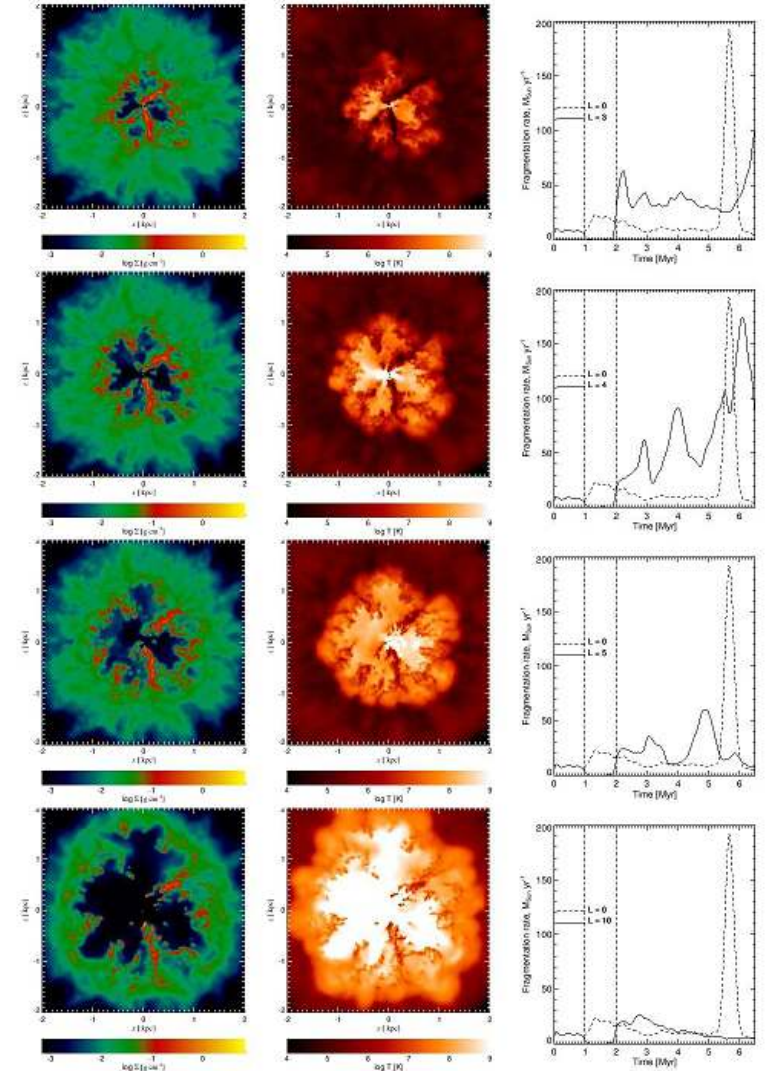
Figure 2. Continuation of Figure 1 for $L = 3, 4, 5, 10$ from top to bottom. Note the different range of temperatures plotted.

MNRAS 000, 000–000 (0000)

Astro-ph:1704.00824

MOLECULAR GAS DOMINATED 50 KPC RAM PRESSURE STRIPPED TAIL OF THE COMA GALAXY D100[*]

PAVEL JÁCHYM[1], MING SUN[2], JEFFREY D. P. KENNEY[3], LUCA CORTESE[4], FRANÇOISE COMBES[5], MASAFUMI YAGI[6,7], MICHITOSHI YOSHIDA[8], JAN PALOUŠ[1], AND ELKE ROEDIGER[9]

Accepted to the Astrophysical Journal on March 31, 2017

ABSTRACT

We have discovered large amounts of molecular gas, as traced by CO emission, in the ram pressure stripped gas tail of the Coma cluster galaxy D100 (GMP 2910), out to large distances of about 50 kpc. D100 has a 60 kpc long, strikingly narrow tail which is bright in X-rays and Hα. Our observations with the IRAM 30m telescope reveal in total $\sim 10^9$ $M_\odot$ of H$_2$ (assuming the standard CO-to-H$_2$ conversion) in several regions along the tail, thus indicating that molecular gas may dominate its mass. Along the tail we measure a smooth gradient in the radial velocity of the CO emission that is offset to lower values from the more diffuse Hα gas velocities. Such a dynamic separation of phases may be due to their differential acceleration by ram pressure. D100 is likely being stripped at a high orbital velocity $\gtrsim 2200$ km s^{-1} by (nearly) peak ram pressure. Combined effects of ICM viscosity and magnetic fields may be important for the evolution of the stripped ISM. We propose D100 has reached a continuous mode of stripping of dense gas remaining in its nuclear region. D100 is the second known
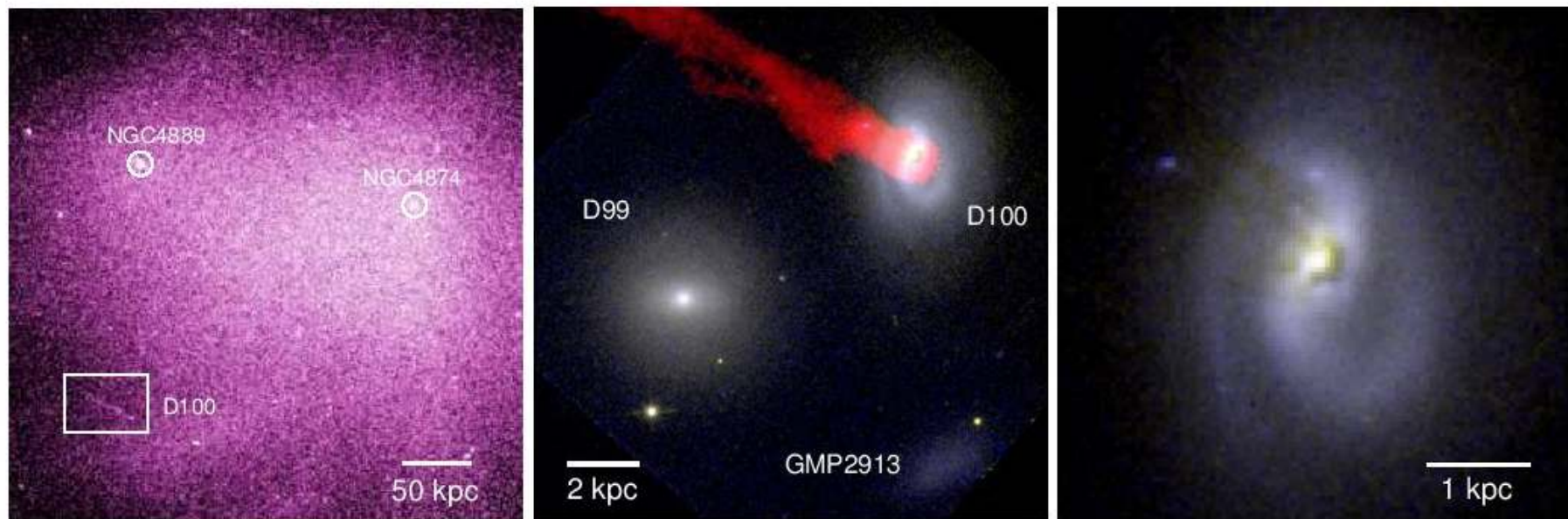
FIG. 1.— Left: *Chandra* view of the central parts of the Coma cluster. Positions of two large elliptical galaxies NGC 4889 and NGC 4874 are shown with circles, together with the position of D100. The remarkable ∼ 48 kpc long X-ray tail extending to the NE direction from D100 is clearly visible. Image credit: NASA/CXC/MPE/Sanders et al. (2013). Middle: HST view of D100's closest neighborhood: projected to the SE is the S0 galaxy D99 (GMP2897) and to the S a weak galaxy GMP2913. The Subaru Hα tail is overlaid in red (Yagi et al. 2010). Right: HST WFPC2 zoom on D100 showing prominent dust extinction filaments extending from the nucleus, as well as two spiral arms and a central bar. The RGB image was created by combining a B (F450W filter, blue), an I (F814W filter, red) and a merged $B + I$ (green) images. A F450W image was already published by Caldwell et al. (1999).

Что за галактика и как наблюдали на IRAM

TABLE 1
PARAMETERS OF THE GALAXY D100 (GMP2910, PGC044716, MRK0060 NED01).

|	
RA, Dec (J2000)	$13^h00^m09^s.14$, $+27°51'59''.2$
type	SBab
redshift[a], V_{helio}	0.01784, 5348 km s^{-1}
V_{Coma}	-1570 km s^{-1}
major diameter (B-band)	24''
major-minor axis ratio	1.35
PA, inclination	178.6°, $\sim 43°$
total B (I) mag	16.09 ± 0.09 (15.23 ± 0.08)
stellar mass[b]	2.1×10^9 $M_\odot$

[a]From Yagi et al. (2007) and corrected from observer's to heliocentric velocity frame.
[b]MEDIAN stellar mass in MPA-JHU SDSS catalog.

TABLE 2
LIST OF OBSERVED POSITIONS.

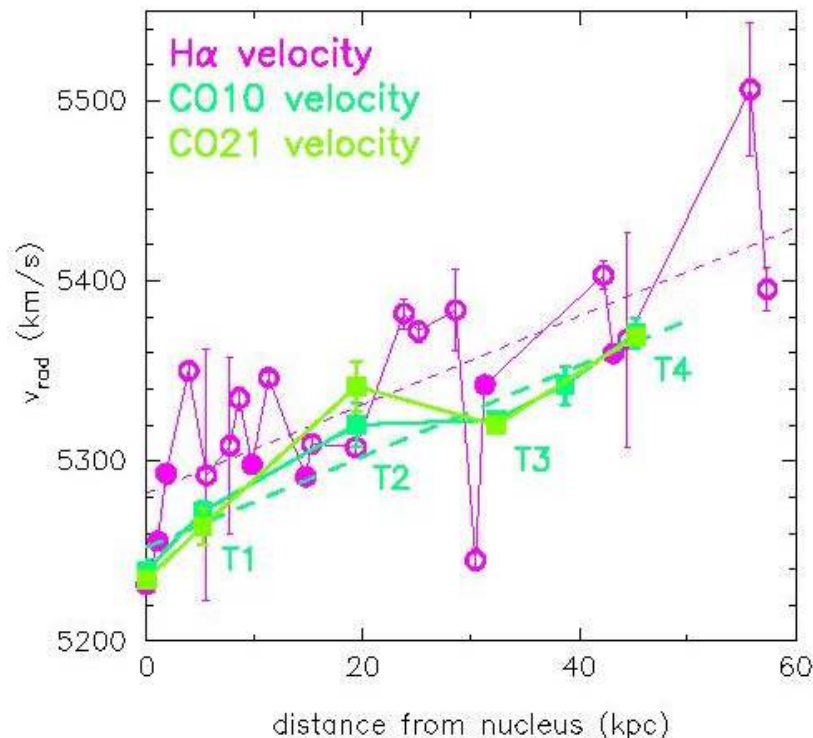|	R.A. (J2000)	Dec. (J2000)	d_{D100} (kpc)	T_{ON} (min)
D100	13:00:09.14	+27:51:59.2	-	99
T1	13:00:09.88	+27:52:04.1	5.2	196
T2	13:00:11.84	+27:52:19.4	19.4	112
TC2	13:00:12.77	+27:52:26.2	26.1	83
T3	13:00:13.64	+27:52:32.4	32.3	127
TC3	13:00:14.53	+27:52:39.0	38.7	106
T4	13:00:15.45	+27:52:45.3	45.2	177

Что увидели
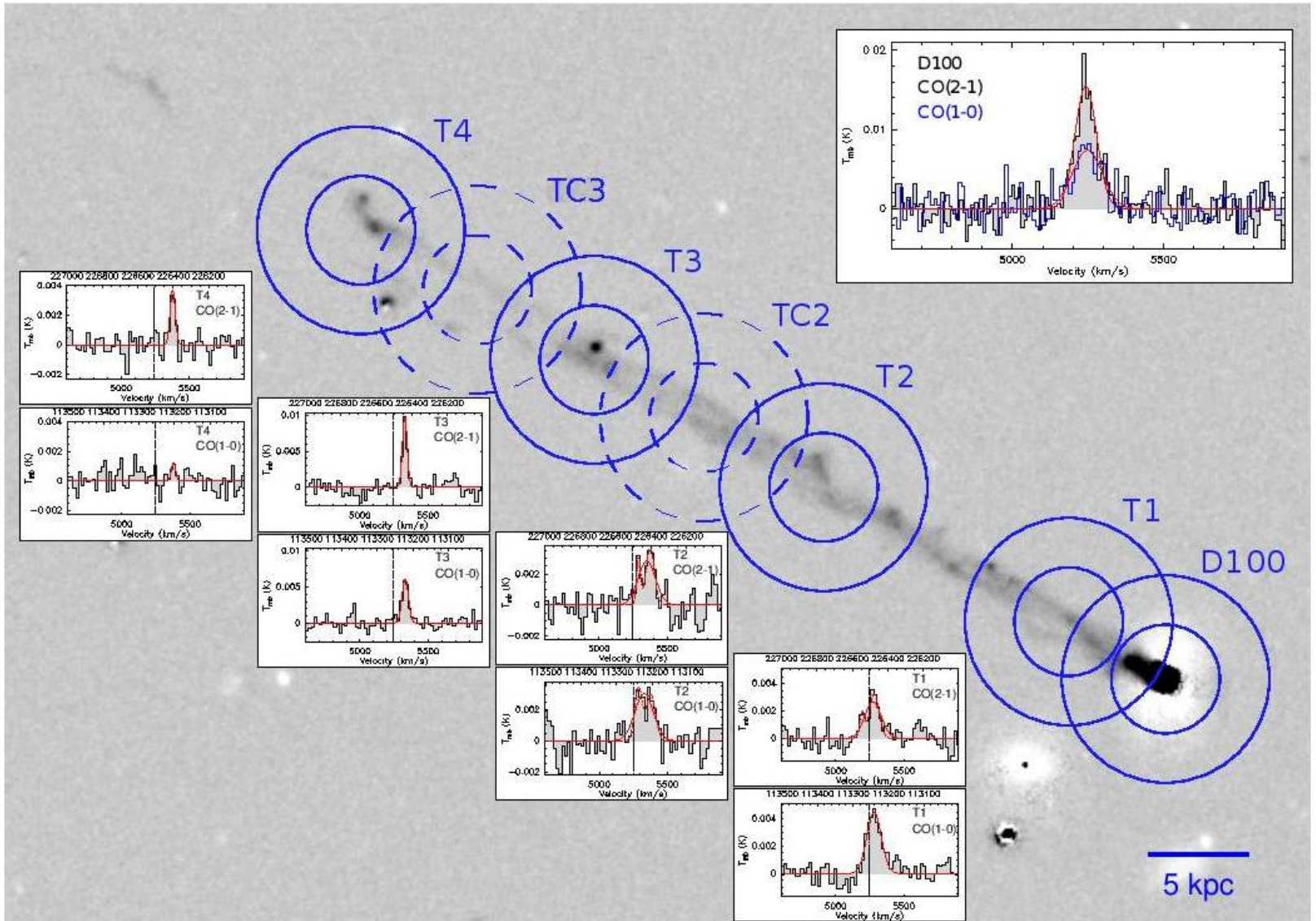
По скоростям молекулярный хвост отстает от H-alpha…

FIG. 6.— Velocity offset between denser, more compact CO and Hα sources and more diffuse Hα warm ionized gas along the D100 tail. Values derived from fitting Hα and [NII] spectral lines (revised from Yagi et al. 2007, converted to radio notation), and CO lines (single fits from Table 3, converted from LSR to heliocentric frame). Dashed lines show linear regression fits to both measurement sets (at distances ≳ 5 kpc). Filled circles indicate compact (possibly H II) regions in the Hα tail, as measured by Hα surface brightness (> 2.1 × 10⁻¹⁷ erg s⁻¹ cm⁻² arcsec⁻²). To estimate Hα velocity
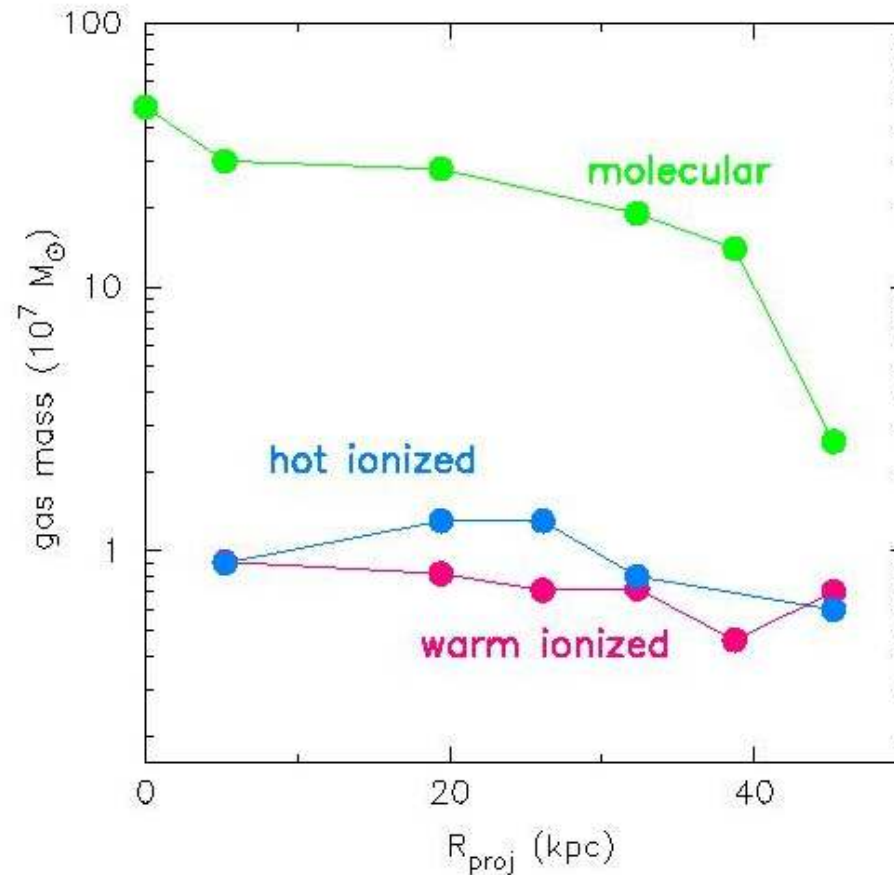
… а по массе - доминирует

FIG. 8.— Masses of individual gas components in the observed regions (IRAM 30m CO(2-1) beams) as a function of projected distance from the galaxy. A volume filling factor of ∼ 0.05 (see e.g., Jáchym et al. 2013) was applied to the ionized gas (Hα) masses.

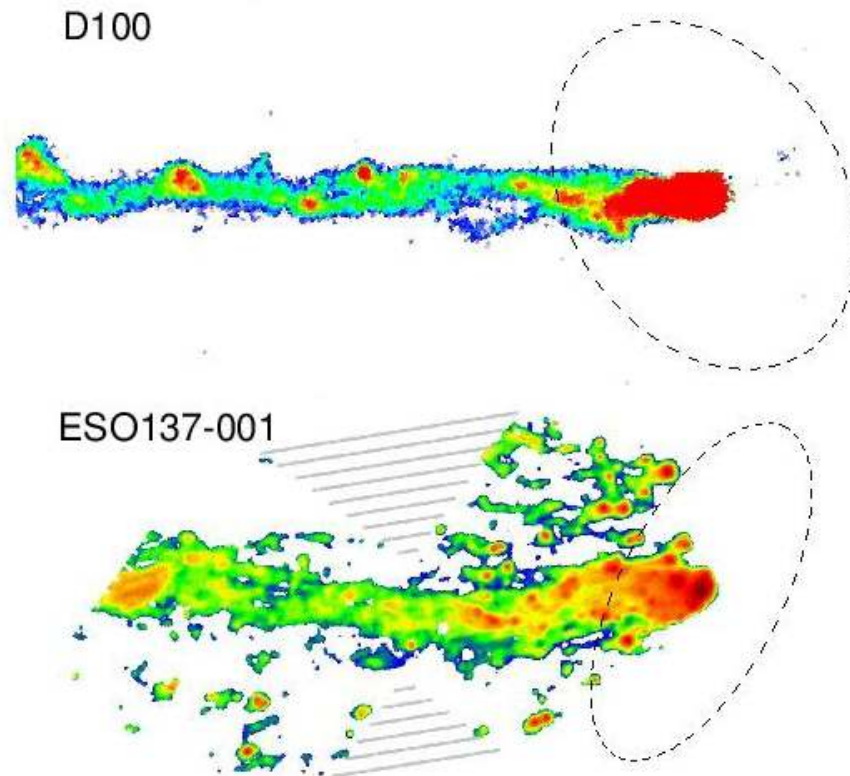# Хвост аномально узкий – без магнитного поля не обойтись!

FIG. 10.— Comparison of inner parts of the tails of D100 (top; Subaru; Yagi et al. 2007) and ESO 137-001 (bottom; MUSE; Fumagalli et al. 2014) as seen in Hα emission. The images are scaled so that the optical diameters of both galaxies are roughly the same (24″ in D100 vs. 75″ in ESO 137-001; marked with dashed ellipses). The striking difference in morphology between the two tails is clearly visible, mainly due to the presence of a broad component in the tail of ESO 137-001. The displayed lengths of the tails correspond to ∼ 20 kpc (D100) and ∼ 40 kpc (ESO 137-001).

Astro-ph:1704.00733

DUST ATTENUATION, BULGE FORMATION AND INSIDE-OUT CESSATION OF STAR-FORMATION IN STAR-FORMING MAIN SEQUENCE GALAXIES AT $Z \sim 2$ [†]

S. Tacchella[1], C. M. Carollo[1], N. M. Förster Schreiber[2], A. Renzini[3,4], A. Dekel[5], R. Genzel[2,6,7], P. Lang[2], S. J. Lilly[1], C. Mancini[3], M. Onodera[8,9], L. J. Tacconi[2], S. Wuyts[10], G. Zamorani[11]

ABSTRACT

We derive two-dimensional dust attenuation maps at ~ 1 kpc resolution from the UV continuum for 10 galaxies on the $z \sim 2$ Star-Forming Main Sequence (SFMS). Comparison with IR data shows that 9 out of 10 galaxies have no further obscuration in addition to the UV-based correction. The individual rest-frame V-band dust attenuation (A_V) radial profiles scatter around an average profile that gently decreases from ~ 1.8 mag in the center down to ~ 0.6 mag at $\sim 3 - 4$ half-mass radii. We use these A_V maps to correct UV- and Hα-based star-formation rates (SFRs), which agree with each other. At masses $\lesssim 10^{11}$ $M_\odot$, the specific SFR (sSFR) profiles are on average radially constant at a mass-doubling timescale of ~ 300 Myr, pointing at a synchronous growth of bulge and disk components in such galaxies. At masses $\gtrsim 10^{11}$ $M_\odot$, the dust-corrected sSFR profiles are typically centrally-suppressed by a factor of ~ 10 relative to the galaxy outskirts. With

Выборка

Table 1

Sample galaxies with Hα redshifts and main stellar population properties.

Source	$z_{H\alpha}$	$M_\star$ $[10^{10}\,M_\odot]$	$(U-V)_{rest}$ [mag]	$A_{V,SED}$ [mag]	$A_{V,map}$ [mag]	SFR_{SED} $[\frac{M_\odot}{yr}]$	SFR_{UV+IR} $[\frac{M_\odot}{yr}]$	Indicator	SFR_{UV} $[\frac{M_\odot}{yr}]$	$SFR_{UV,map}$ $[\frac{M_\odot}{yr}]$
ZC400569	2.241	23.3	1.29	1.4	1.5	241.0	239.3	UV+24μm	168.0	156.6
ZC400528	2.387	16.0	0.84	0.9	0.5	148.0	556.5	UV+100μm	148.0	46.7
Q2343-BX610	2.211	15.5	0.93	0.8	1.2	60.0	—	—	60.0	85.5
D3A15504	2.383	15.0	0.71	1.0	1.0	150.2	145.6	UV+24μm	150.0	116.1
ZC406690	2.195	5.3	0.56	0.7	1.0	200.0	296.5	UV+24μm	337.0	201.2
ZC407302	2.182	2.98	0.50	1.3	0.6	340.0	358.1†	UV+24μm	130.0	67.0
ZC412369	2.028	2.86	0.88	1.0	1.3	94.1	IR-undet	—	130.0	140.2
Q2346-BX482	2.257	2.5	0.77	0.8	1.1	79.8	—	—	80.0	95.8
ZC405226	2.287	1.13	0.56	1.0	0.9	117.0	IR-undet	—	87.0	58.3
ZC405501	2.154	1.04	0.33	0.9	0.6	84.9	IR-undet	—	68.0	28.1

Note. — Listed are the Hα spectroscopic redshifts from the AO SINFONI data ($z_{H\alpha}$), the stellar masses ($M_\star$; defined as the integral of the SFR), the rest frame $U-V$ colors, the dust attenuation $A_{V,SED}$ from galaxy-integrated SED modelling, the dust attenuation $A_{V,map}$ from the $(FUV-NUV)$ color maps, the SFRs from SED (SFR_{SED}), the UV+IR SFRs (SFR_{UV+IR}), the SFR indicator of the IR, SFR from the integrated UV photometry (SFR_{UV}), and the SFR from the UV maps ($SFR_{UV,map}$). For the SED modeling we use Bruzual & Charlot (2003) model and assume a Chabrier (2003) IMF, solar metallicity, the Calzetti et al. (2000) reddening law, and either constant or exponentially declining SFRs. The uncertainties on the stellar properties are dominated by systematics from the model assumption and are up to a factor of $\sim 2-3$ for $M_\star$ and ~ 3 or more for SFRs. Sources undetected with Spitzer/MIPS and Herschel/PACS are indicated explicitly with 'IR-undet', to distinguish them from objects in fields without MIPS and PACS observations.
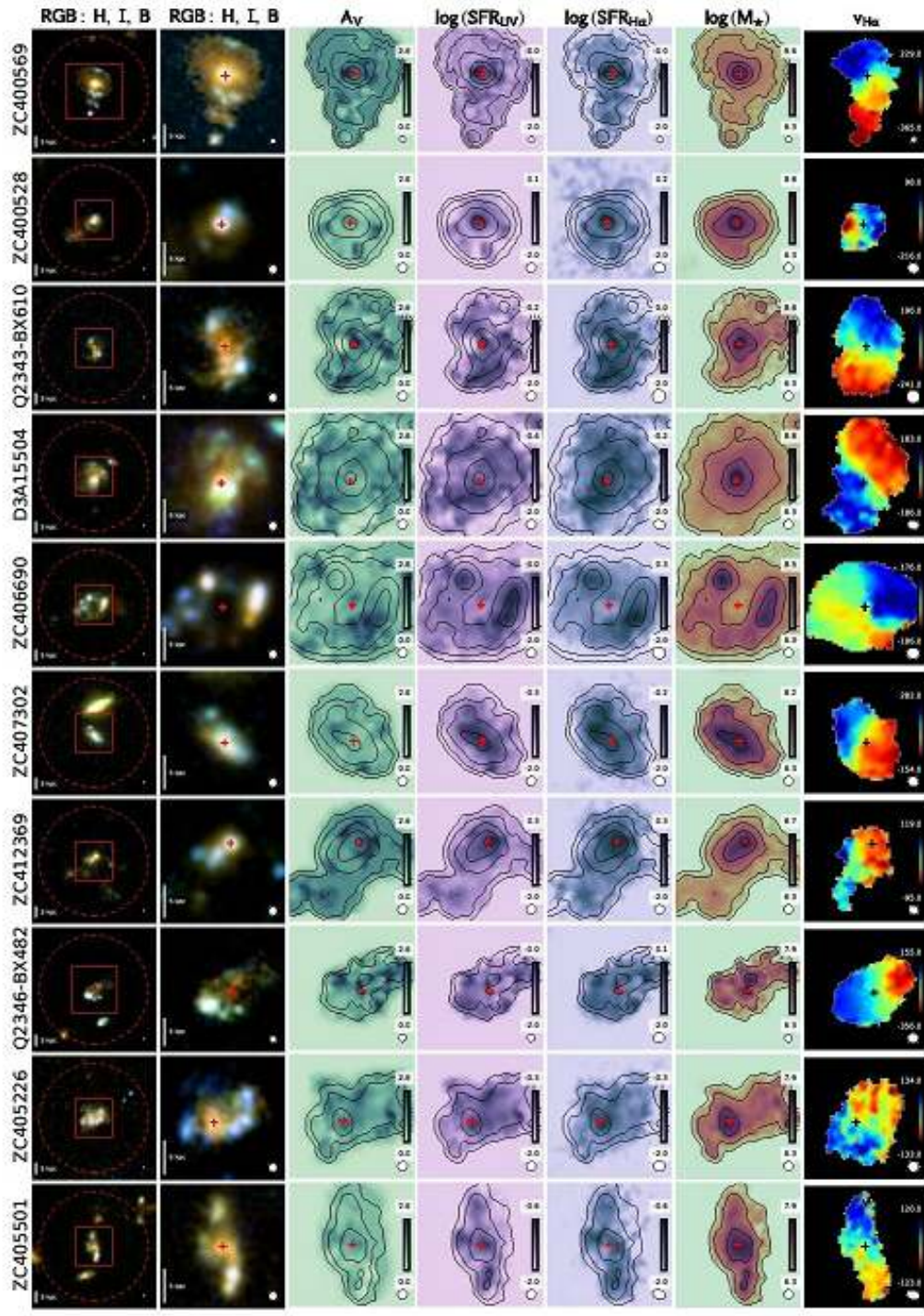
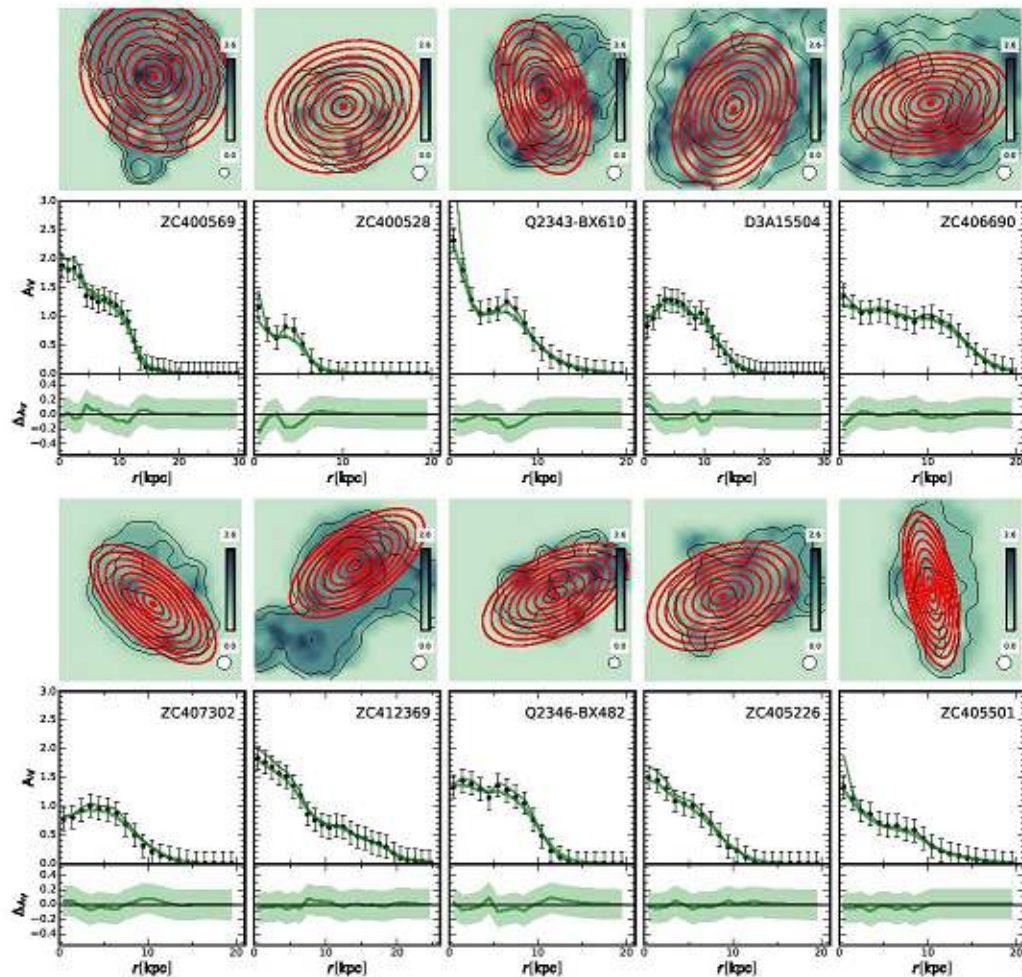# Карты поглощения, полученные по FUV-NUV (restframe)

Figure 5. Derivation of the azimuthally averaged dust attenuation A_V profiles. For each galaxy, the top panel shows the A_V map. The red ellipses show the apertures used to construct the azimuthally averaged profile and the contours show the mass distribution. The middle panels show the A_V profiles: the data points with error bars indicate the measured values directly from the A_V map, while the thin and thick green lines show the PSF-corrected and PSF-convolved profiles, respectively. The bottom panels show the difference between the data and the PSF-convolved profiles. The PSF-corrected profiles describe the data well with less than 0.2 mag difference, which is within the estimated uncertainty.

Средние профили поглощения – все, как ожидалось
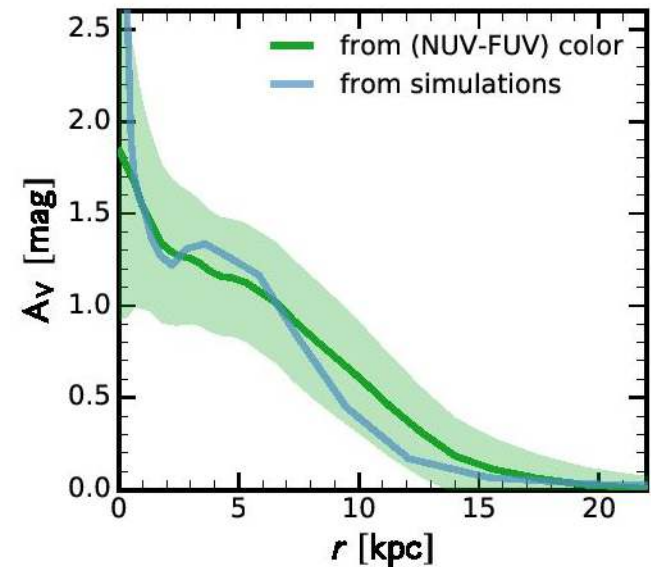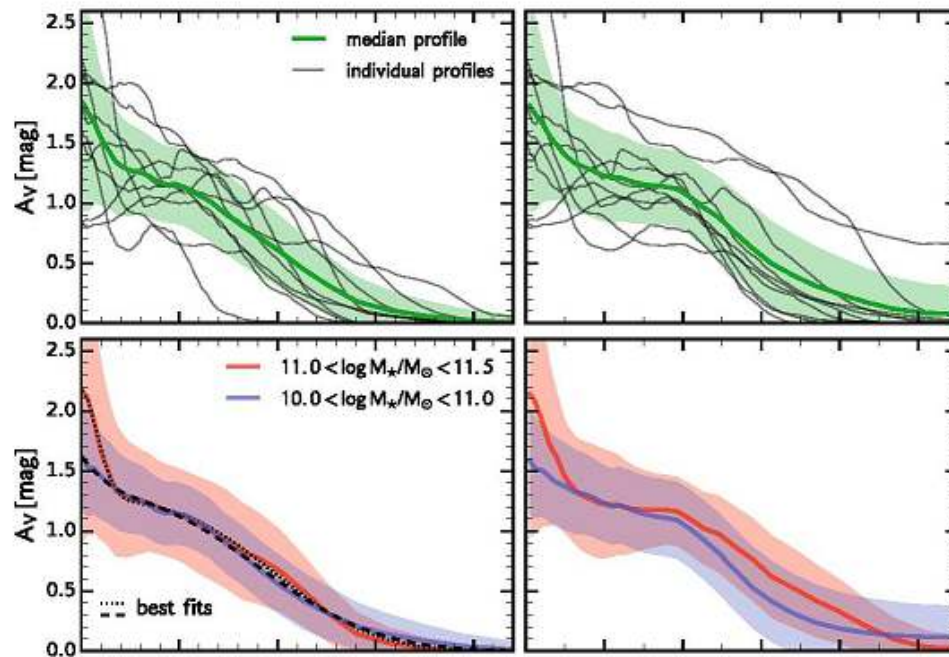
Figure 7. Comparison of our average A_V profile measured from the (FUV−NUV) color (green line) with the A_V profiles derived from gas surface density profiles in cosmological zoom-in simulations (blue line). There is an overall good agreement between observations and simulations within the scatter.

А это уже радиальные профили темпов звездообразования…
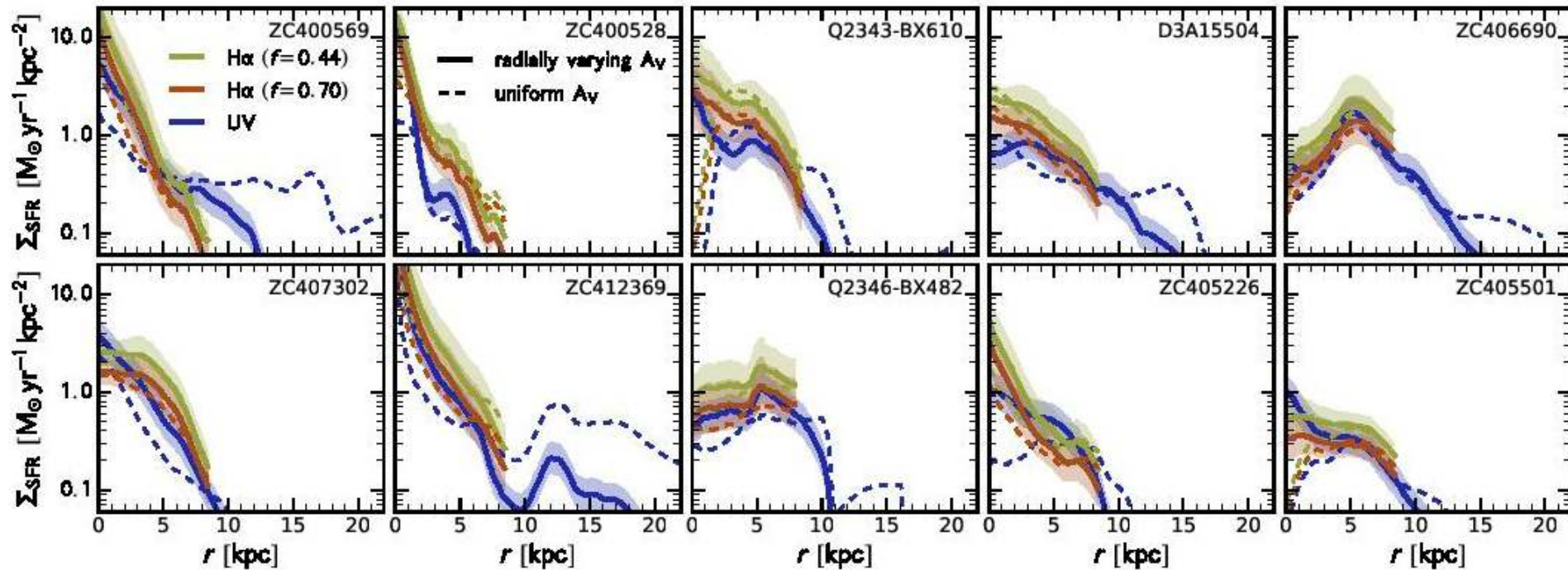
Figure 8. Radial SFR surface density profiles. Each panel shows the profiles for an individual galaxy. The khaki, red and blue line indicate the SFR estimated from Hα with $f = 0.44$, Hα with $f = 0.70$, and UV, respectively. The dashed and solid lines show the SFR profiles assuming a uniform dust screen and the radial A_V profiles from Figure 6, respectively. The UV and Hα (especially with $f = 0.70$) SFR profiles agree within the uncertainty. Our galaxies have SFR densities in their centers of $0.3 - 20 \ M_\odot \ \mathrm{yr}^{-1} \ \mathrm{kpc}^{-2}$. Several galaxie

У массивных галактик «специфическое» SF подавлено в центре
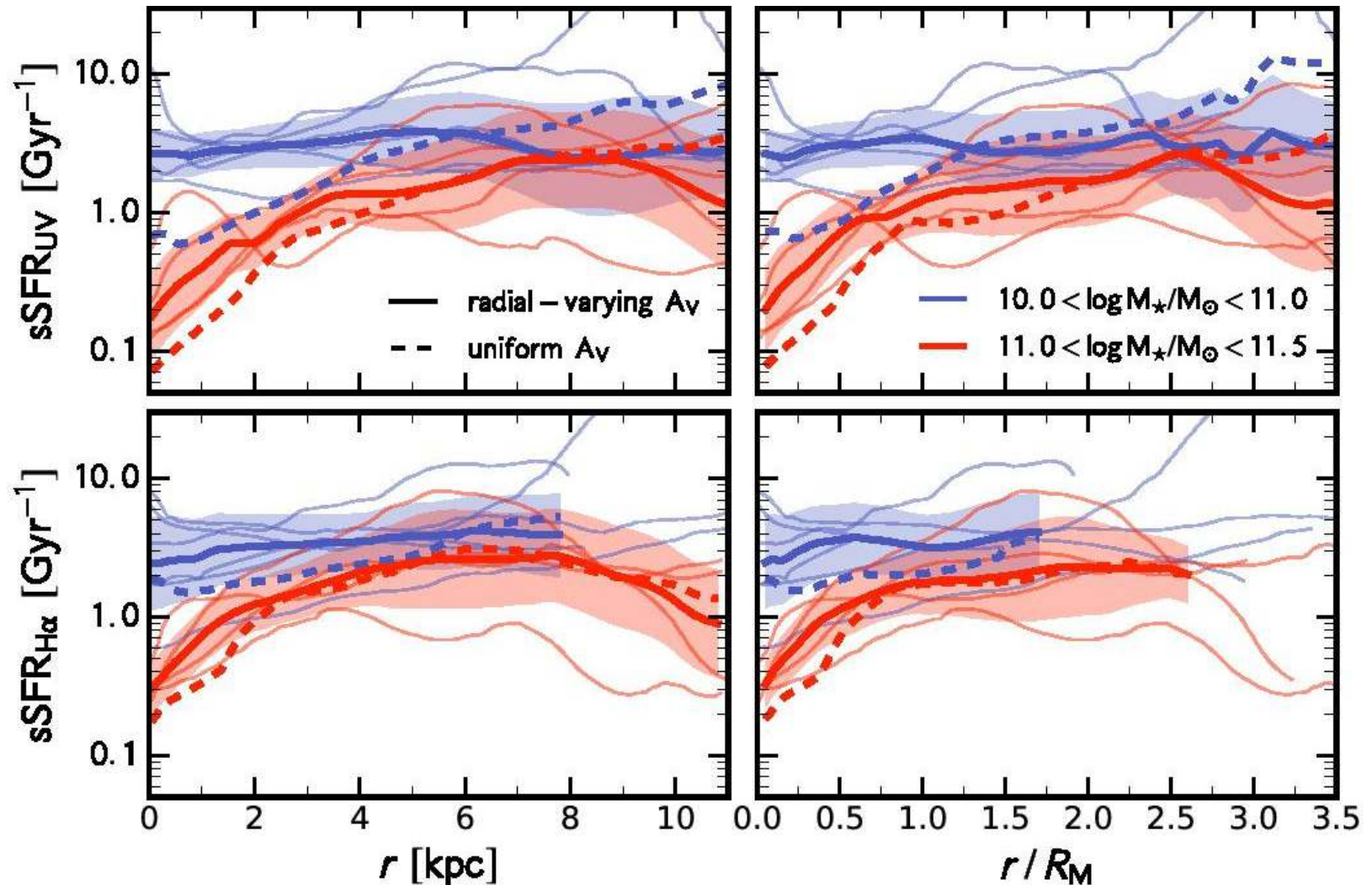
Путешествие поперек «главной последовательности»?
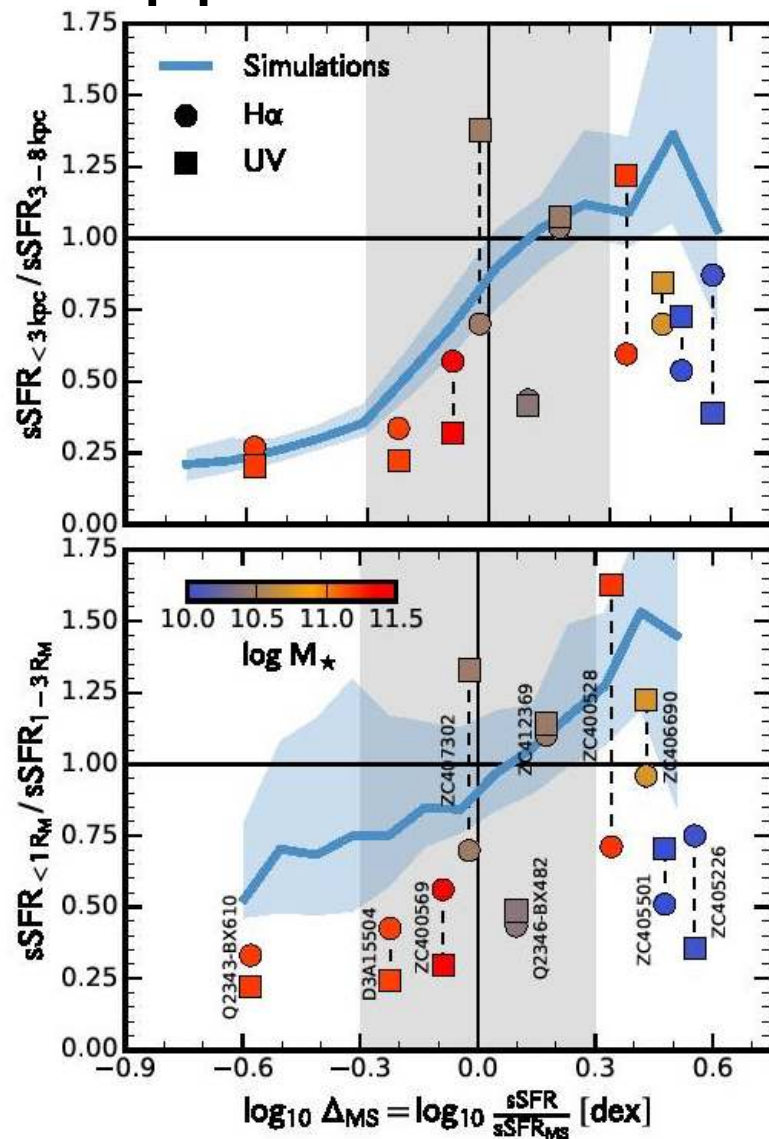
THE SAMI GALAXY SURVEY: MASS AS THE DRIVER OF THE KINEMATIC MORPHOLOGY – DENSITY RELATION IN CLUSTERS

Sarah Brough,[1,2,3] Jesse van de Sande,[4] Matt S. Owers,[2,5] Francesco d'Eugenio,[3,6] Rob Sharp,[6] Luca Cortese,[7] Nicholas Scott,[3,4] Scott M. Croom,[3,4] Rob Bassett,[7] Kenji Bekki,[7] Julia J. Bryant,[2,3,4] Roger Davies,[8] Michael J. Drinkwater,[3,9] Simon P. Driver,[7] Caroline Foster,[2] Gregory Goldstein,[5] Á. R. López-Sánchez,[2,5] Anne M. Medling,[6,10,11] Sarah M. Sweet,[12] Dan S. Taranu,[3,7] Chiara Tonini,[13] Sukyoung K. Yi,[14] Michael Goodwin,[2] J. S. Lawrence,[2] and Samuel N. Richards[2,3,4]

[1] School of Physics, University of New South Wales, NSW 2052, Australia
[2] Australian Astronomical Observatory, 105 Delhi Rd, North Ryde, NSW 2113, Australia
[3] ARC Centre of Excellence for All-sky Astrophysics (CAASTRO)
[4] Sydney Institute for Astronomy (SIfA), School of Physics, The University of Sydney, NSW 2006, Australia
[5] Department of Physics and Astronomy, Macquarie University, NSW 2109, Australia
[6] Research School of Astronomy and Astrophysics, Australian National University, Canberra, ACT 2611, Australia
[7] International Centre for Radio Astronomy Research (ICRAR), University of Western Australia, 35 Stirling Highway, Crawley, WA 6009, Australia
[8] Astrophysics, Department of Physics, University of Oxford, Denys Wilkinson Building, Keble Rd., Oxford, OX1 3RH, UK
[9] School of Mathematics and Physics, University of Queensland, QLD 4072, Australia
[10] Cahill Center for Astronomy and Astrophysics, California Institute of Technology, MS 249-17 Pasadena, CA 91125, USA
[11] Hubble Fellow
[12] Centre for Astrophysics and Supercomputing, Swinburne University of Technology, PO Box 218, Hawthorn, VIC 3122, Australia
[13] School of Physics, Melbourne University, Parkville, VIC 3010 Australia
[14] Department of Astronomy and Yonsei University Observatory, Yonsei University, Seoul 120-749, Republic of Korea

Выборка скоплений SAMI

Table 1. The properties of the eight galaxy clusters observed by SAMI. N_{Mem} is the number of members within $1R_{200}$ and $\pm 3.5 V_{cl}/\sigma_{cl}$. N_{ETG} is the number of early-type members with $\log M_*/M_\odot \geq 10$ (ETGs). N_{Obs} is the number of observed ETGs. N_λ is the number of observed ETGs for which the spin parameter could be measured. $Comp_{ETG,\lambda}$ gives the fraction of ETGs with spin parameter measurements. N_{SPS} gives the number of SAMI Pilot Survey galaxies added to the analysis (Section 4.2.2).

Cluster	R.A. J2000	Dec J2000	z_{cl}	M_{200} $\log(M_\odot)$	R_{200} Mpc	N_{Mem}	N_{ETG}	N_{Obs}	N_λ	$Comp_{ETG,\lambda}$	N_{SPS}
EDCC0442	6.38068	-33.04657	0.0498	14.45	1.41	50	39	32	30	0.77	0
Abell0085	10.460211	-9.303184	0.0549	15.19	2.42	167	133	62	55	0.41	12
Abell0119	14.06715	-1.25537	0.0442	14.92	2.02	253	132	61	52	0.39	0
Abell0168	18.815777	0.213486	0.0449	14.28	1.33	112	51	21	21	0.41	7
Abell2399	329.389487	-7.794236	0.0579	14.66	1.63	92	68	50	46	0.68	3
Abell3880	336.97705	-30.575371	0.0578	14.64	1.62	56	42	24	24	0.57	0
APMCC0917	355.39788	-29.236351	0.0509	14.26	1.19	29	23	18	15	0.65	0
Abell4038	356.93781	-28.140661	0.0293	14.36	1.46	89	35	29	28	0.8	0
Total:	-	-	-	-	-	848	523	297	271	0.52	22

# Главная формула для современной версии диаграммы Бинни-Корменди!

4.2. Spin parameter

Emsellem et al. (2007) defined the luminosity-weighted, spin parameter (λ_R):

$$\lambda_R = \frac{\sum_{i=0}^{i=N} F_i R_i |V_i|}{\sum_{i=0}^{i=N} F_i R_i \sqrt{V_i^2 + \sigma_i^2}}, \qquad (1)$$

in this analysis R_i is the major axis of the ellipse in which spaxel i is located and F_i is the flux of the ith spaxel in units of erg cm^2 s^{-1} Å^{-1}. λ_R is summed over all spaxels, N, that meet the stellar kinematics quality cut described above within an ellipse of semi-major axis

А вот и сама диаграмма Бинни-Корменди
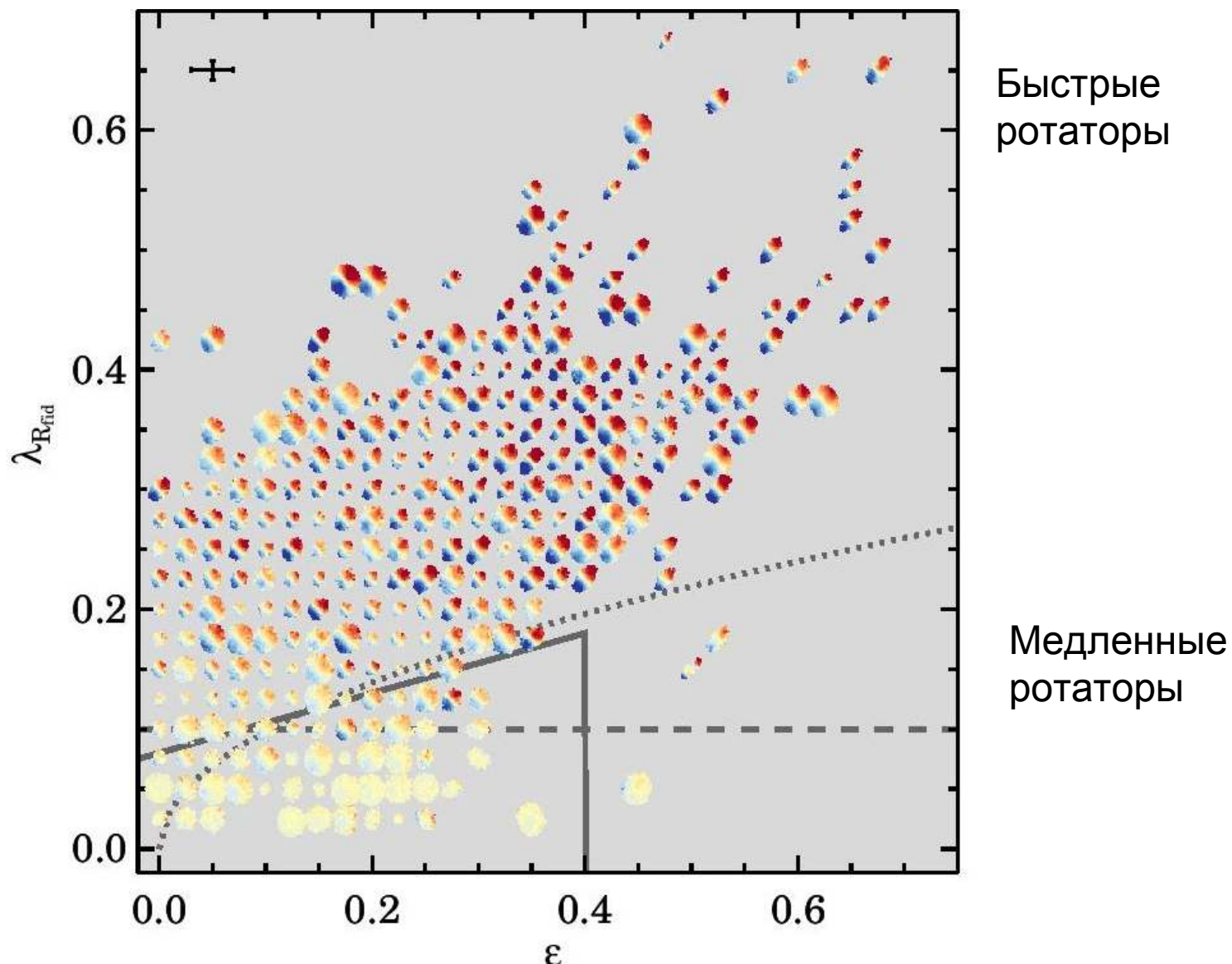
# Доля медленных ротаторов сильнее всего зависит от массы ГАЛАКТИКИ
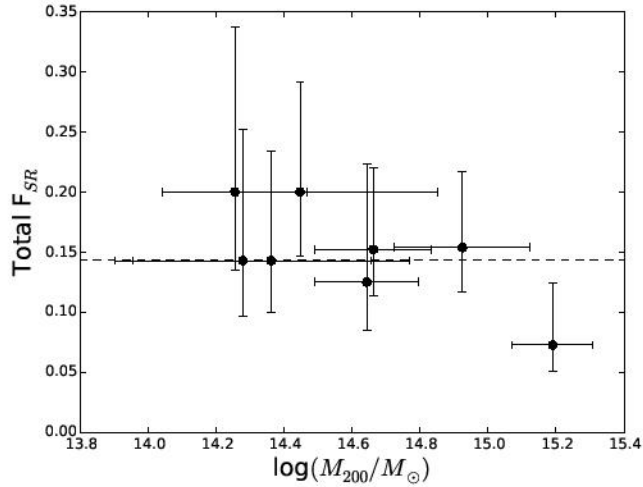
Figure 6. Total fraction of slow rotators, F_{SR}, as a function of host cluster mass, M_{200}. The dashed line shows the total fraction of slow rotators across our whole sample. The uncertainties are the fractional uncertainties. We find no relationship of total F_{SR} with host cluster mass over this mass range.
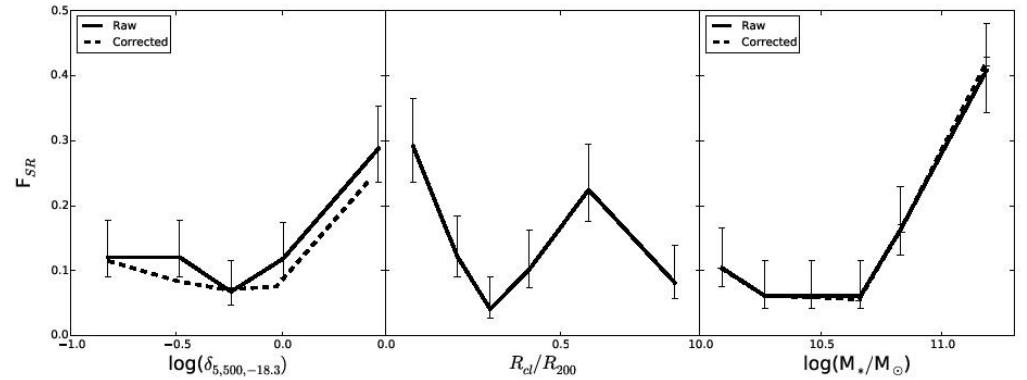
Figure 7. Fraction of slow rotators, F_{SR}. The left-hand panel shows F_{SR} as a function of environmental overdensity, $\delta_{5,500,-18.3}$. The solid line gives the observed data, while the dashed line indicates the results of testing the effect of higher SAMI observing completeness at higher stellar masses. Stellar mass completeness does not have a significant effect on the $F_{SR}-\delta_{5,500,-18.3}$ relation. We observe an increasing fraction of slow rotators with increasing overdensity. The middle panel shows F_{SR} as a function of stacked cluster-centric distance, R_{cl}/R_{200}. The fraction of slow rotators increases with decreasing cluster-centric radius. Interestingly there is a 'bump' at $R_{cl}/R_{200} \sim 0.6$ due to substructure in four of the clusters. The right-hand panel shows F_{SR} as a function of stellar mass, M_*. The solid line gives the observed data, while the dashed line indicates the results of testing the effect of higher SAMI observing completeness at higher stellar masses. Stellar mass completeness does not have a significant effect on the $F_{SR}-M_*$ relation. We observe that the fraction of slow rotators increases with increasing stellar mass.

А вот если зависимость от массы галактики вычесть – то уходит зависимость от плотности окружения
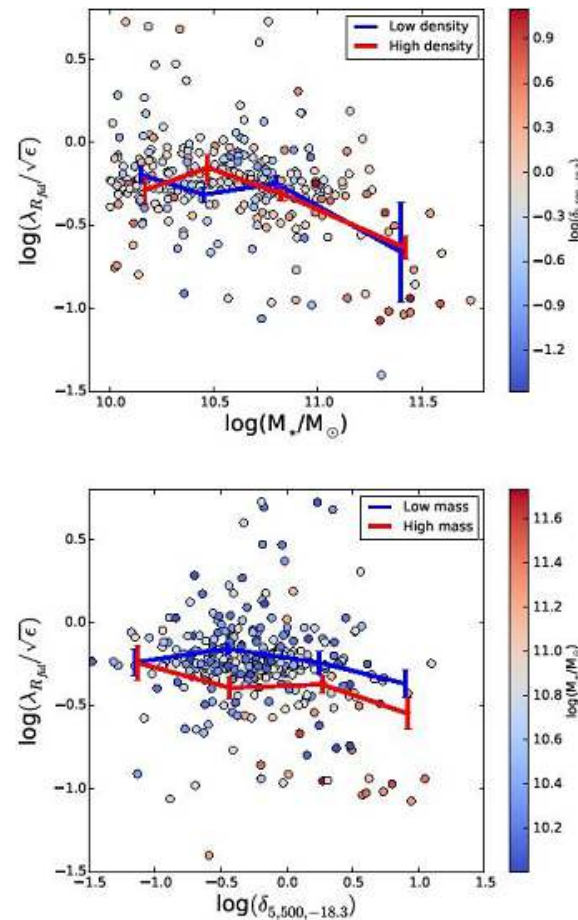
Figure 10. The upper panel shows the distribution of corrected spin parameter, $\lambda_{R_{fid}}/\sqrt{\epsilon}$, as a function of stellar mass, M_*, with colors showing environment overdensity, $\delta_{5,500,-18.3}$. The lines show mean $\lambda_{R_{fid}}/\sqrt{\epsilon}$ as a function of stellar mass for the lower and upper quartiles of overdensity. $\lambda_{R_{fid}}/\sqrt{\epsilon}$ does depend on stellar mass but that rela-

Выводы – четкие и с размахом

mass. We draw the following conclusions that are not qualitatively dependent on fiducial radius or choice of fast/slow galaxy classification:

- We find a total slow rotator fraction of $F_{SR} = 0.14 \pm 0.02$.

- The slow rotator fraction per cluster shows no dependence on host cluster mass in the range studied.

- We find F_{SR} to depend on local cluster environment such that it increases with increasing environmental overdensity, from $F_{SR} = 0.14^{+0.05}_{-0.03}$ at $\log(\delta) \sim -0.9$ to $F_{SR} = 0.20^{0.06}_{-0.05}$ at $\log(\delta) \sim 0.4$, a significance of 3.4σ.

- F_{SR} depends more strongly on stellar mass than on local cluster environment. The fraction of slow rotators increases with increasing stellar mass from $F_{SR} = 0.13^{+0.06}_{-0.03}$ at $\log(M_*/M_\odot) \sim 10.1$ to $F_{SR} = 0.41^{0.07}_{-0.06}$ at $\log(M_*/M_\odot) \sim 11.2$, a significance of 5.0σ.

- Once any dependence on stellar mass is removed from the distribution of spin parameter, $\lambda_{R_{fid}}/\sqrt{\epsilon}$, no significant relationship with local cluster environment remains.

We conclude that the cluster kinematic morphology–density relationship is a result of mass segregation due to dynamical friction. We will test this hypothesis further with the broader SAMI Galaxy Survey sample (van de